Spitzer Microlensing Parallax Reveals Two Isolated Stars in the Galactic Bulge

Journal Item

How to cite:

Zang, Weicheng; Shvartzvald, Yossi; Wang, Tianshu; Udalski, Andrzej; Lee, Chung-Uk; Sumi, Takahiro; Skottfelt, Jesper; Li, Shun-Sheng; Mao, Shude; Zhu, Wei; Yee, Jennifer C.; Calchi Novati, Sebastiano; Beichman, Charles A.; Bryden, Geoffery; Carey, Sean; Gaudi, B. Scott; Henderson, Calen B.; Mróz, Przemek; Skowron, Jan; Poleski, Radoslaw; Szymański, Michał K.; Soszyński, Igor; Pietrukowicz, Paweł; Kozłowski, Szymon; Ulaczyk, Krzysztof; Rybicki, Krzysztof A.; Iwanek, Patryk; Bachelet, Etienne; Christie, Grant; Green, Jonathan; Hennerley, Steve; Maoz, Dan; Natusch, Tim; Pogge, Richard W.; Street, Rachel A.; Tsapras, Yiannis; Albrow, Michael D.; Chung, Sun-Ju; Gould, Andrew; Han, Cheongho; Hwang, Kyu-Ha; Jung, Youn Kil; Ryu, Yoon-Hyun; Shin, In-Gu; Cha, Sang-Mok; Kim, Dong-Jin; Kim, Hyoun-Woo; Kim, Seung-Lee; Lee, Dong-Joo; Lee, Yongseok; Park, Byeong-Gon; Bond, Ian A.; Abe, Fumio; Barry, Richard; Bennett, David P.; Bhattacharya, Aparna; Donachie, Martin; Fukui, Akihiko; Hirao, Yuki; Itow, Yoshitaka; Kondo, Iona; Koshimoto, Naoki; Alex Li, Man Cheung; Matsubara, Yutaka; Muraki, Yasushi; Miyazaki, Shota; Nagakane, Masayuki; Ranc, Clément; Rattenbury, Nicholas J.; Suematsu, Haruno; Sullivan, Denis J.; Suzuki, Daisuke; Tristram, Paul J.; Yonehara, Atsunori; Dominik, Martin; Hundertmark, Markus; Jørgensen, Uffe G.; Rahvar, Sohrab; Sajadian, Sedighe; Snodgrass, Colin; Bozza, Valerio; Burgdorf, Martin J.; Evans, Daniel F.; Jaimes, R. Figuera; Fujii, Yuri I.; Mancini, Luigi; Longa-Peña, Penelope; Helling, Christiane; Peixinho, Nuno; Rabus, Markus; Southworth, John; Unda-Sanzana, Eduardo and Essen, Carolina von (2020). Spitzer Microlensing Parallax Reveals Two Isolated Stars in the Galactic Bulge. The Astrophysical Journal, 891(1), article no. 3.

Version: Accepted Manuscript

Link(s) to article on publisher's website:
http://dx.doi.org/doi:10.3847/1538-4357/ab6ff8

Draft version April 26, 2019
Typeset using LaTeX **twocolumn** style in AASTeX62

Spitzer Microlensing parallax reveals two isolated stars in the Galactic bulge

Weicheng Zang,[1] Yossi Shvartzvald,[2] Tianshu Wang,[1] Andrzej Udalski,[3] Chung-Uk Lee,[4,5] Takahiro Sumi,[6]
Jesper Skottfelt,[7] Shun-Sheng Li,[8,9] Shude Mao,[1,8] and Wei Zhu[10]
—
Jennifer C. Yee,[11] Sebastiano Calchi Novati,[2] Charles A. Beichman,[2] Geoffery Bryden,[12] Sean Carey,[2]
B. Scott Gaudi,[13] and Calen B. Henderson[2]
(The *Spitzer* Team)
Przemek Mróz,[3] Jan Skowron,[3] Radoslaw Poleski,[3,13] Michał K. Szymański,[3] Igor Soszyński,[3] Paweł Pietrukowicz,[3]
Szymon Kozłowski,[3] Krzysztof Ulaczyk,[14] Krzysztof A. Rybicki,[3] and Patryk Iwanek[3]
(The OGLE Collaboration)
Etienne Bachelet,[15] Grant Christie,[16] Jonathan Green,[17] Steve Hennerley,[17] Dan Maoz,[18] Tim Natusch,[16,19]
Richard W. Pogge,[13,20] Rachel A. Street,[15] and Yiannis Tsapras[21]
(The LCO and μFUN Follow-up Teams)
Michael D. Albrow,[22] Sun-Ju Chung,[4,23] Andrew Gould,[4,13,24] Cheongho Han,[25] Kyu-Ha Hwang,[4] Youn Kil Jung,[26,4]
Yoon-Hyun Ryu,[4] In-Gu Shin,[4] Sang-Mok Cha,[4,27] Dong-Jin Kim,[4] Hyoun-Woo Kim,[4] Seung-Lee Kim,[4,23]
Dong-Joo Lee,[4] Yongseok Lee,[4,27] Byeong-Gon Park,[4,23] and Richard W. Pogge[13]
(The KMTNet Collaboration)
Ian A. Bond,[28] Fumio Abe,[29] Richard Barry,[30] David P. Bennett,[30,31] Aparna Bhattacharya,[30,31] Martin Donachie,[32]
Akihiko Fukui,[33] Yuki Hirao,[6] Yoshitaka Itow,[29] Iona Kondo,[6] Naoki Koshimoto,[34,35] Man Cheung Alex Li,[32]
Yutaka Matsubara,[29] Yasushi Muraki,[29] Shota Miyazaki,[6] Masayuki Nagakane,[6] Clément Ranc,[30]
Nicholas J. Rattenbury,[32] Haruno Suematsu,[6] Denis J. Sullivan,[36] Daisuke Suzuki,[37] Paul J. Tristram,[38] and
Atsunori Yonehara[39]
(The MOA Collaboration)
Martin Dominik,[40] Markus Hundertmark,[21] Uffe G. Jørgensen,[41] Sohrab Rahvar,[42] Sedighe Sajadian,[43]
Colin Snodgrass,[44] Valerio Bozza,[45,46] Martin J. Burgdorf,[47] Daniel F. Evans,[48] Roberto Figuera Jaimes,[21]
Yuri I. Fujii,[41,49] Luigi Mancini,[50,51,52] Penelope Longa-Peña,[53] Christiane Helling,[40] Nuno Peixinho,[54]
Markus Rabus,[55,56] John Southworth,[48] Eduardo Unda-Sanzana,[53] and Carolina von Essen[57]
(The MiNDSTEp Collaboration)

[1] *Physics Department and Tsinghua Centre for Astrophysics, Tsinghua University, Beijing 100084, China*
[2] *IPAC, Mail Code 100-22, Caltech, 1200 E. California Blvd., Pasadena, CA 91125, USA*
[3] *Warsaw University Observatory, Al. Ujazdowskie 4, 00-478 Warszawa, Poland*
[4] *Korea Astronomy and Space Science Institute, Daejon 34055, Republic of Korea*
[5] *University of Science and Technology, Korea, (UST), 217 Gajeong-ro Yuseong-gu, Daejeon 34113, Republic of Korea*
[6] *Department of Earth and Space Science, Graduate School of Science, Osaka University, Toyonaka, Osaka 560-0043, Japan*
[7] *Centre for Electronic Imaging, Department of Physical Sciences, The Open University, Milton Keynes, MK7 6AA, UK*
[8] *National Astronomical Observatories, Chinese Academy of Sciences, Beijing 100101, China*
[9] *School of Astronomy and Space Science, University of Chinese Academy of Sciences, Beijing 100049, China*
[10] *Canadian Institute for Theoretical Astrophysics, University of Toronto, 60 St George Street, Toronto, ON M5S 3H8, Canada*
[11] *Center for Astrophysics — Harvard & Smithsonian, 60 Garden St.,Cambridge, MA 02138, USA*
[12] *Jet Propulsion Laboratory, California Institute of Technology, 4800 Oak Grove Drive, Pasadena, CA 91109, USA*
[13] *Department of Astronomy, Ohio State University, 140 W. 18th Ave., Columbus, OH 43210, USA*
[14] *Department of Physics, University of Warwick, Gibbet Hill Road, Coventry, CV4 7AL, UK*
[15] *Las Cumbres Observatory, 6740 Cortona Drive, suite 102, Goleta, CA 93117, USA*
[16] *Auckland Observatory, Auckland, New Zealand*
[17] *Kumeu Observatory, Kumeu, New Zealand*
[18] *School of Physics and Astronomy, Tel-Aviv University, Tel-Aviv 6997801, Israel*
[19] *Institute for Radio Astronomy and Space Research (IRASR), AUT University, Auckland, New Zealand*
[20] *Center for Cosmology & AstroParticle Physics, The Ohio State University, 191 West Woodruff Avenue, Columbus, OH 43210*
[21] *Astronomisches Rechen-Institut, Zentrum für Astronomie der Universität Heidelberg (ZAH), 69120 Heidelberg, Germany*

Corresponding author: Weicheng Zang
zangwc17@mails.tsinghua.edu.cn

[22]University of Canterbury, Department of Physics and Astronomy, Private Bag 4800, Christchurch 8020, New Zealand
[23]Korea University of Science and Technology, 217 Gajeong-ro, Yuseong-gu, Daejeon 34113, Republic of Korea
[24]Max-Planck-Institute for Astronomy, Königstuhl 17, 69117 Heidelberg, Germany
[25]Department of Physics, Chungbuk National University, Cheongju 28644, Republic of Korea
[26]Harvard-Smithsonian Center for Astrophysics, 60 Garden St.,Cambridge, MA 02138, USA
[27]School of Space Research, Kyung Hee University, Yongin, Kyeonggi 17104, Republic of Korea
[28]Institute of Natural and Mathematical Sciences, Massey University, Auckland 0745, New Zealand
[29]Institute for Space-Earth Environmental Research, Nagoya University, Nagoya 464-8601, Japan
[30]Code 667, NASA Goddard Space Flight Center, Greenbelt, MD 20771, USA
[31]Department of Astronomy, University of Maryland, College Park, MD 20742, USA
[32]Department of Physics, University of Auckland, Private Bag 92019, Auckland, New Zealand
[33]Okayama Astrophysical Observatory, National Astronomical Observatory of Japan, 3037-5 Honjo, Kamogata, Asakuchi, Okayama 719-0232, Japan
[34]Department of Astronomy, Graduate School of Science, The University of Tokyo, 7-3-1 Hongo, Bunkyo-ku, Tokyo 113-0033, Japan
[35]National Astronomical Observatory of Japan, 2-21-1 Osawa, Mitaka, Tokyo 181-8588, Japan
[36]School of Chemical and Physical Sciences, Victoria University, Wellington, New Zealand
[37]Institute of Space and Astronautical Science, Japan Aerospace Exploration Agency, 3-1-1 Yoshinodai, Chuo, Sagamihara, Kanagawa, 252-5210, Japan
[38]University of Canterbury Mt. John Observatory, P.O. Box 56, Lake Tekapo 8770, New Zealand
[39]Department of Physics, Faculty of Science, Kyoto Sangyo University, 603-8555 Kyoto, Japan
[40]Centre for Exoplanet Science, SUPA, School of Physics & Astronomy, University of St Andrews, North Haugh, St Andrews KY16 9SS, UK
[41]Niels Bohr Institute & Centre for Star and Planet Formation, University of Copenhagen, Øster Voldgade 5, 1350 Copenhagen, Denmark
[42]Department of Physics, Sharif University of Technology, PO Box 11155-9161 Tehran, Iran
[43]Department of Physics, Isfahan University of Technology, Isfahan 84156-83111, Iran
[44]School of Physical Sciences, Faculty of Science, Technology, Engineering and Mathematics, The Open University, Walton Hall, Milton Keynes, MK7 6AA, UK
[45]Dipartimento di Fisica "E.R. Caianiello", Università di Salerno, Via Giovanni Paolo II 132, 84084, Fisciano, Italy
[46]Istituto Nazionale di Fisica Nucleare, Sezione di Napoli, Napoli, Italy
[47]Universität Hamburg, Faculty of Mathematics, Informatics and Natural Sciences, Department of Earth Sciences, Meteorological Institute, Bundesstraße 55, 20146 Hamburg, Germany
[48]Astrophysics Group, Keele University, Staffordshire, ST5 5BG, UK
[49]Institute for Advanced Research, Nagoya University, Furo-cho, Chikusa-ku, Nagoya, 464-8601, Japan
[50]Max Planck Institute for Astronomy, Königstuhl 17, 69117 Heidelberg, Germany
[51]Dipartimento di Fisica, Universit di Roma Tor Vergata, Via della Ricerca Scientifica 1, I-00133Roma, Italy
[52]International Institute for Advanced Scientific Studies (IIASS), Via G. Pellegrino 19, I-84019, Vietri sul Mare (SA), Italy
[53]Centro de Astronomía (CITEVA), Universidad de Antofagasta, Avda. U. de Antofagasta 02800, Antofagasta, Chile
[54]CITEUC – Center for Earth and Space Research of the University of Coimbra, Geophysical and Astronomical Observatory, R. Observatório s/n, 3040-004 Coimbra, Portugal
[55]Las Cumbres Observatory Global Telescope, 6740 Cortona Dr., Suite 102, Goleta, CA 93111, USA
[56]Department of Physics, University of California, Santa Barbara, CA 93106-9530, USA
[57]Stellar Astrophysics Centre, Department of Physics and Astronomy, Aarhus University, Ny Munkegade 120, 8000 Aarhus C, Denmark

ABSTRACT

We report the mass and distance measurements of two single-lens events from the 2017 *Spitzer* microlensing campaign. The ground-based observations yield the detection of finite-source effects, and the microlens parallaxes are derived from the joint analysis of ground-based observations and *Spitzer* observations. We find that the lens of OGLE-2017-BLG-1254 is a $0.60 \pm 0.03 M_{\odot}$ star with $D_{\rm LS} = 0.53 \pm 0.11$ kpc, where $D_{\rm LS}$ is the distance between the lens and the source. The second event, OGLE-2017-BLG-1161, is subject to the known satellite parallax degeneracy, and thus is either a $0.51^{+0.12}_{-0.10} M_{\odot}$ star with $D_{\rm LS} = 0.40 \pm 0.12$ kpc or a $0.38^{+0.13}_{-0.12} M_{\odot}$ star with $D_{\rm LS} = 0.53 \pm 0.19$ kpc. Both of the lenses are therefore isolated stars in the Galactic bulge. By comparing the mass and distance distributions of the eight published *Spitzer* finite-source events with the expectations from a Galactic model, we find that the *Spitzer* sample is in agreement with the probability of finite-source effects occurrence in single lens events.

1. INTRODUCTION

Gravitational microlensing opens a powerful window for probing isolated objects with various masses such as free-floating planets, brown dwarfs, low-mass stars and black holes. At the low-mass end, microlensing has detected several free-floating planet candidates (Sumi et al. 2011; Mróz et al. 2017, 2018, 2019), including a few possible Earth-mass objects. Such discoveries are crucial for testing theories about the origin and evolution of free-floating planets (Ma et al. 2016; Clanton & Gaudi 2017; Veras & Raymond 2012;

Pfyffer et al. 2015; Barclay et al. 2017). For more massive objects (i.e., isolated brown dwarfs), five have been discovered by microlensing: OGLE-2007-BLG-224L (Gould et al. 2009), OGLE-2015-BLG-1268L (Zhu et al. 2016), OGLE-2015-BLG-1482[1] (Chung et al. 2017), OGLE-2017-BLG-0896 (Shvartzvald et al. 2019), and OGLE-2017-BLG-1186 [2] (Li et al. 2019). Shvartzvald et al. (2019) recently announced the discovery of an isolated, extremely low-mass brown dwarf of $M \sim 19 M_J$, with proper motion in the opposite direction of disk stars, which indicates that it might be a halo brown dwarf or from a different, unknown counter-rotating population. At the high-mass end, Gould (2000b) estimated that $\sim 20\%$ of microlensing events observed toward the Galactic bulge are caused by stellar remnants, and specifically that $\sim 1\%$ are due to stellar-mass black holes, with another $\sim 3\%$ due to neutron star lenses. The first observed example of this was the long-timescale (~ 640 day) event OGLE-1999-BUL-32, for which the microlens parallax measurement indicated this event could be a stellar black hole (Mao et al. 2002). In addition, Wyrzykowski et al. (2016) identified 13 microlensing events that are consistent with having a white-dwarf, neutron-star or a black-hole lens in the OGLE-III data base.

In general, for microlensing events due to isolated lenses, the only measured parameter that describes the physical properties of the lens system is the Einstein timescale $t_{\rm E}$. Because $t_{\rm E}$ depends on the lens mass, the distances to the lens and source, and the transverse velocity (See Equation 17 of Mao 2012), it can only be used to make a statistical estimate of the lens mass. Unambiguous measurements of the lens mass requires two second-order microlensing observables: the angular Einstein radius $\theta_{\rm E}$ and the microlens parallax $\pi_{\rm E}$. For a lensing object, the total mass is related to the two observables by (Gould 1992, 2000a)

$$M_{\rm L} = \frac{\theta_{\rm E}}{\kappa \pi_{\rm E}}, \tag{1}$$

and its distance by

$$D_{\rm L} = \frac{\rm au}{\pi_{\rm rel} + \pi_{\rm S}}, \qquad \pi_{\rm rel} = \pi_{\rm E}\theta_{\rm E} \tag{2}$$

where $\kappa \equiv 4G/(c^2{\rm AU}) = 8.144\ {\rm mas}/M_\odot$, $\pi_{\rm S} = {\rm au}/D_{\rm S}$ is the source parallax, $D_{\rm S}$ is the source distance (Gould 1992, 2004) and $\pi_{\rm rel}$ is the lens-source relative parallax.

There are three methods to measure the microlens parallax $\pi_{\rm E}$. The first one is "orbital microlens parallax", which can be measured when including the orbital motion of Earth around the Sun in modeling (Gould 1992; Alcock et al. 1995). However, this method is generally feasible only for events with long microlensing timescales $t_{\rm E} \gtrsim {\rm year}/2\pi$ (e.g., Udalski et al. 2018). The second method, "terrestrial microlens parallax", in rare cases can be measured by a combination of simultaneous observations from ground-based telescopes that are well separated (e.g., Gould et al. 2009; Yee et al. 2009). The most efficient and robust method to measure the microlens parallax is to simultaneously observe an event from Earth and a satellite (Refsdal 1966; Gould 1994). That is the "satellite microlens parallax". The feasibility of satellite microlens parallax measurements has been demonstrated by *Spitzer* microlensing programs (Dong et al. 2007; Udalski et al. 2015b; Yee et al. 2015b; Zhu et al. 2015; Calchi Novati et al. 2015a). Since 2014, the *Spitzer* satellite has observed more than 700 microlensing events toward the Galactic bulge, yielding the mass measurements of eight isolated lens objects (Zhu et al. 2016; Chung et al. 2017; Shin et al. 2018; Shvartzvald et al. 2019; Li et al. 2019), including two in this work.

For the measurements of the angular Einstein radius $\theta_{\rm E}$, Dong et al. (2019) recently reported the angular Einstein radius $\theta_{\rm E}$ measurement of microlensing event TCP J05074264+2447555 by interferometric resolution of the microlensed images. However, this method requires a rare, bright microlensing event (for TCP J05074264+2447555, $K \sim 10.6$ mag at the time of observation). Measurements of the angular Einstein radius $\theta_{\rm E}$ are obtained primarily via finite-source effects and an estimate of the angular diameter θ_* of the source from its de-reddened color and magnitude (e.g., Kervella & Fouqué 2008; Boyajian et al. 2014)

$$\theta_{\rm E} = \frac{\theta_*}{\rho}, \tag{3}$$

where ρ is the source size normalized by the Einstein radius, which can be measured from the modulation in the lensing light curve with finite-source effects. Such effects arise when the source transits a caustic (where the magnification diverges to infinity) or comes close to a cusp (Gould 1994; Witt & Mao 1994; Nemiroff & Wickramasinghe 1994). Then the source cannot be regarded as a point-like source, and the observed magnification is the integration of the magnification pattern over the face of the source. Finite-source effects are frequently measured in binary/planetary events, for which the caustic structures are relatively large, but they are rarely measured in the case of a single lens event because the caustic is a single geometric point.

Here we present the mass and distance measurements of two *Spitzer* single-lens microlensing events OGLE-2017-BLG-1161 and OGLE-2017-BLG-1254. The ground-based observations yield a robust detection of finite-source effects for the two events, and the microlens parallaxes are derived from the joint analysis of ground-based observations and

---

[1] OGLE-2015-BLG-1482 has two possible solutions, with $M = 55 \pm 9 M_J$ or $M = 96 \pm 23 M_J$.

[2] OGLE-2017-BLG-1186 has two possible solutions, with $M = 45 \pm 1 M_J$ or $M = 73 \pm 2 M_J$.

Spitzer observations. Combining the measurements of $\theta_{\rm E}$ and $\pi_{\rm E}$, we find that the lenses of the two events are both isolated stars in the Galactic bulge. The paper is structured as follows. In Section 2, we introduce ground-based and *Spitzer* observations of the two events. We then describe the light curve modeling process in Section 3, and present the physical parameters of the two events in Section 4. Finally, our conclusions and the implications of our work are given in Section 5.

2. OBSERVATIONS AND DATA REDUCTIONS

The observations of OGLE-2017-BLG-1161 and OGLE-2017-BLG-1254 both consist of *Spitzer*, ground-based survey and ground-based follow-up observations.

The *Spitzer* observations were part of a large program to measure the Galactic distribution of planets in different stellar environments (Calchi Novati et al. 2015a; Zhu et al. 2017). The detailed protocols and strategies for the *Spitzer* observations are discussed in Yee et al. (2015a). Specifically, the two events were observed by the *Spitzer* satellite because they were both high-magnification events, which are more sensitive to planets (Griest & Safizadeh 1998). The *Spitzer* observations were taken using the 3.6 μm channel ($L-$band) of the IRAC camera.

Ground-based surveys included the Optical Gravitational Lensing Experiment (OGLE, Udalski et al. 2015a), the Microlensing Observations in Astrophysics (MOA, Sumi et al. 2016), and the Korea Microlensing Telescope Network (KMTNet, Kim et al. 2016). OGLE is in its fourth phase (OGLE-IV), and the observations are carried out using its 1.3 m Warsaw Telescope equipped with a 1.4 $\rm deg^2$ FOV mosaic CCD camera at the Las Campanas Observatory in Chile. The MOA group conducts a high cadence survey toward the Galactic bulge using its 1.8 m telescope equipped with a 2.2 $\rm deg^2$ FOV camera at the Mt. John University Observatory in New Zealand. KMTNet consists of three 1.6 m telescopes, equipped with 4 $\rm deg^2$ FOV cameras at the Cerro Tololo International Observatory (CTIO) in Chile (KMTC), the South African Astronomical Observatory (SAAO) in South Africa (KMTS), and the Siding Spring Observatory (SSO) in Australia (KMTA). The majority of observations were taken in the I-band for the OGLE and KMTNet groups, and the MOA-Red filter (which is similar to the sum of the standard Cousins R- and I-band filters) for the MOA group, with occasional observations taken in the V-band.

The aim of the ground-based follow-up observations was to detect and characterize any planetary signatures with dense observations, which are crucial if an event is not heavily monitored by the ground-based surveys (e.g., OGLE-2017-BLG-1161) or the ground-based surveys could not observe due to weather (e.g., OGLE-2016-BLG-1045 Shin et al. 2018). The follow-up teams included the Las Cumbres Observatory (LCO) global network, the Microlensing Follow-Up Network (μFUN, Gould et al. 2010) and Microlensing Network for the Detection of Small Terrestrial Exoplanets (MiNDSTEp, Dominik et al. 2010). The LCO global network provided observations from its 1.0m telescopes located at CTIO, SAAO and SSO, with the SDSS-i' filter. The μFUN team followed the events using the 1.3m SMARTS telescope at CTIO (CT13) with V/I/H-bands (DePoy et al. 2003), the 0.4m telescope at Auckland Observatory (AO) using a number 12 Wratten filter (which is similar to R-band), and the 0.36m telescope at Kumeu Observatory (Kumeu) in Auckland. The MiNDSTEp team monitored the events using the Danish 1.54-m telescope sited at ESOs La Silla observatory in Chile, with a non-standard filter.

We provide detailed descriptions of the observations for OGLE-2017-BLG-1161 and OGLE-2017-BLG-1254 in the next part.

2.1. *OGLE-2017-BLG-1161*

OGLE-2017-BLG-1161 was discovered by the OGLE collaboration on 2017 June 20. With equatorial coordinates $(\alpha,\delta)_{\rm J2000}$ = (17:41:12.65, $-$26:44:28.1) and Galactic coordinates $(\ell,b) = (1.36,1.98)$, it lies in OGLE field BLG652, monitored by OGLE with a cadence of 0.5–1 observations per night (Udalski et al. 2015a). This event was located in the gap of two CCD chips of KMTNet BLG15 field, and thus the follow-up observations were important supplements to the sparse observations from the ground-based surveys. The I/H-band observations from CT13 intensively covered the falling side of the peak, and its H-band data were also used to derive the color of the source because this event suffered from very high extinction ($A_I \sim 4.5$; See Section 4). In addition, OGLE-2017-BLG-1161 was also densely observed by the LCO network, the 0.4 m telescope at Auckland Observatory (AO), and the 0.36m telescope at Kumeu Observatory (Kumeu). OGLE-2017-BLG-1161 was selected as a "secret" *Spitzer* target on 2017 June 25 (UT 16:00) because the newest OGLE point (HJD = 2457932.78) indicated a significant rise (consistent with a high-magnification event) and the event was predict to peaked within 1 day, and it was formally announced as a *Spitzer* target on 2017 June 28. The *Spitzer* observations began on 2017 June 30 and ended on 2017 July 13 with 16 data points in total.

2.2. *OGLE-2017-BLG-1254*

OGLE-2017-BLG-1254 was first alerted by the OGLE collaboration on 2017 July 2. The event was located at equatorial coordinates $(\alpha,\delta)_{\rm J2000}$ = (17:57:23.56, $-$27:13:13.3), corresponding to Galactic coordinates $(\ell,b) = (2.80$,-1.36$)$. It therefore lies in OGLE field BLG645, which has a cadence less than 0.5 observations per night (Udalski et al. 2015a). This event was also identified by MOA group as MOA-2017-

BLG-373 ∼12.2 days later (Bond et al. 2001), and recognized by KMTNet's event-finding algorithm as KMT-2017-BLG-0374 (Kim et al. 2018). The KMTNet group observed this event in its two slightly offset fields BLG02 and BLG42, with combined cadence of $\Gamma = 4\ \mathrm{hr}^{-1}$. The LCO, μFUN, and MiNDSTEp follow-up teams also observed this event. The dense observations during the peak by LCO and MiNDSTEp were important to constrain the finite-source effects. The H-band observations taken by CT13 were important for characterizing the source star because this event suffered from very high extinction ($A_I \sim 4.2$; See Section 4). OGLE-2017-BLG-1254 was chosen as a "secret" *Spitzer* target on 2017 July 2 (UT 20:48) because (1) the model predicted that the event could be a high-magnification event; (2) KMTNet has a high cadence of $\Gamma = 4\ \mathrm{hr}^{-1}$. It was "subjectively" selected on July 6 and became "objective" on July 17 (see Yee et al. 2015a). The *Spitzer* observations began on 2017 July 7 and ended on 2017 August 3 with a cadence of ~ 1 observation per day.

2.3. *Data Reductions*

The photometry of OGLE, MOA, KMTNet, LCO, AO, Kumeu, and Danish data was extracted using custom implementations of the difference image analysis technique (Alard & Lupton 1998): Wozniak 2000 (OGLE), Bond et al. 2001 (MOA), Albrow et al. 2009 (KMTNet, LCO, AO, and Kumeu), and Bramich 2008 (Danish). In addition, the CT13 data were reduced by `DoPHOT` (Schechter et al. 1993). The *Spitzer* data were reduced using the algorithm developed by Calchi Novati et al. (2015b) for crowded-field photometry.

3. LIGHT CURVE ANALYSIS

3.1. *Ground-based data only*

For each event, we model the ground-based data using four parameters for the magnification, $A(t)$. These include three Paczyński parameters (t_0, u_0, t_E) (Paczyński 1986) to describe the light curve produced by a single-lens with a point-source: the time of the maximum magnification as seen from Earth t_0, the impact parameter u_0 (in units of the angular Einstein radius θ_E), and the Einstein radius crossing time t_E. In addition, the source size normalized by the angular Einstein radius ρ is needed to incorporate finite-source effects. The flux, $f(t)$, calculated from the model is

$$f(t) = f_\mathrm{s} A(t) + f_\mathrm{b}, \tag{4}$$

where f_s represents the flux of the source star being lensed, and f_b is any blended flux that is not lensed. The two linear parameters, f_s and f_b, are different for each observatory and each filter. In addition, we adopt the linear limb-darkening law to consider the brightness profile of the source star (An et al. 2002)

$$S_\lambda(\theta) = \bar{S}_\lambda \left[1 - \Gamma_\lambda (1 - \frac{3}{2}\cos\theta)\right], \tag{5}$$

where $\bar{S}_\lambda$ is the mean surface brightness of the source, θ is the angle between the normal to the surface of the source and the line of sight, and Γ_λ is the limb-darkening coefficient at wavelength λ. We employ the Markov chain Monte Carlo (MCMC) χ^2 minimization using the `emcee` ensemble sampler (Foreman-Mackey et al. 2013) to find the best-fit parameters and their uncertainties.

3.2. *Satellite parallax*

We measure the microlens parallax from the light curve modeling,

$$\vec{\pi}_\mathrm{E} \sim \frac{\mathrm{AU}}{D_\perp}\left(\Delta u_0, \frac{\Delta t_0}{t_\mathrm{E}}\right), \tag{6}$$

where Δt_0 is the difference in event peak time t_0 and Δu_0 is the difference in impact parameter u_0 as seen from the *Spitzer* satellite and Earth, and $D_\perp$ is the projected separation between the *Spitzer* satellite and Earth at the time of the event. Generally, only the absolute value of u_0 can be measured from the modeling, and thus the satellite parallax measurements usually suffer from a four-fold degeneracy (Refsdal 1966; Gould 1994). We specify the four solutions as $(+,+)$, $(+,-)$, $(-,-)$, and $(-,+)$ using the sign convention described in Zhu et al. (2015). Briefly, the first and second signs in each parenthesis indicate the signs of $u_{0,\oplus}$ and $u_{0,Spitzer}$, respectively. In addition, the *Spitzer* observations only cover the falling part of OGLE-2017-BLG-1161 which leads to large uncertainty of π_E. Thus, we include a color-color constraint on the *Spitzer* source flux $f_{s,Spitzer}$ to improve the parallax measurement (e.g. Calchi Novati et al. 2015a). This constraint adds a χ^2_penalty into the total χ^2 (See Equation (2) in Shin et al. 2017 for the form of the χ^2_penalty).

3.3. *OGLE-2017-BLG-1161*

Using the intrinsic color of the source star (see Section 4.1) and the color-temperature relation of Houdashelt et al. (2000), we estimate the effective temperature of the source to be $T_\mathrm{eff} \approx 4450$ K. Applying ATLAS models and assuming a surface gravity of $\log g = 2.5$, a metallicity of [M/H] = 0.0, and a microturbulence parameter of $1\ \mathrm{km\,s^{-1}}$, we obtain the linear limb-darkening coefficients $u_I = 0.60$ for I band, $u_V = 0.81$ for V band, $u_R = 0.71$ for R band, $u_H = 0.39$ for H band, and $u_L = 0.24$ for L band (Claret & Bloemen 2011). We then employ the transformation formula in Fields et al. (2003), yielding the corresponding limb-darkening coefficients $\Gamma_I = 0.50, \Gamma_V = 0.74, \Gamma_R = 0.62, \Gamma_H = 0.30$, and $\Gamma_L = 0.18$. In the light curve modeling, we use Γ_I for OGLE, LCO, CT13 $I-$band and Kumeu data, $\Gamma_\mathrm{AO} = (\Gamma_V + \Gamma_R)/2 = 0.68$ for AO data, Γ_H for CT13 $H-$band data, and Γ_L for *Spitzer* data.

To derive the color-color constraint on the *Spitzer* source flux $f_{s,Spitzer}$, we extract the *Spitzer* photometry of red giant bulge stars ($4.0 < I_\mathrm{OGLE} - H_\mathrm{VVV} < 5.5; 17.5 < I_\mathrm{OGLE} <$

20.0) and fit for the two parameters in the equation

$$I_{\rm OGLE} - L_{Spitzer} = c_0 + c_1(I_{\rm OGLE} - H_{\rm VVV} - X_p), \quad (7)$$

where $X_p = 4.65$ is a pivot parameter chosen to minimize the covariance between the parameters. We then obtain $c_0 = 4.47 \pm 0.01, c_1 = 1.28 \pm 0.03$. This, when combined with $(I_{\rm OGLE} - H_{\rm VVV})_{\rm S} = 4.71 \pm 0.01$ (see Section 4.1), yields $(I_{\rm OGLE} - L_{Spitzer})_{\rm S} = 4.55 \pm 0.02$. We employ this constraint on the light curve modeling.

Table 1 shows the best-fit parameters and their 1σ uncertainties for the four-fold degenerate solutions ($\Delta\chi^2 < 0.16$). The best-fit model curves for the $(-,+)$ solution are shown in Figure 1. For all the four-fold degenerate solutions, the East component $\pi_{\rm E,E}$ of the microlens parallax vector is $\sim 0.038 \pm 0.06$, while the North component $\pi_{\rm E,N}$ is consistent with 0 at the $\sim 2\sigma$ level.

3.4. *OGLE-2017-BLG-1254*

Applying the same procedure as in Section 3.3, we obtain the corresponding limb-darkening coefficients $\Gamma_I = 0.45, \Gamma_R = 0.55, \Gamma_H = 0.26$, and $\Gamma_L = 0.16$. In the light curve modeling, we use Γ_I for OGLE, KMTNet, LCO, CT13 $I-$band and Danish data, $\Gamma_{\rm MOA} = (\Gamma_I + \Gamma_R)/2 = 0.50$ for MOA data, Γ_H for CT13 $H-$band data, and Γ_L for *Spitzer* data. We find that the impact parameter $u_{0,\oplus} \simeq 0$, so the four degenerate solutions reduce to two solutions $[(0,+),(0,-)]$, with $\Delta\chi^2 = 0.09$. However, this degeneracy has no effect on the mass and distance measurement for the lens (Gould & Yee 2012; Shin et al. 2018). The best-fit model curves for $(0,+)$ are shown in Figure 2, and the best-fit parameters for the two degenerate solutions are shown in Table 1.

For this event the *Spitzer* light curve precisely constrains the microlens parallax without the need of color-color constraint on $L_{Spitzer}$. Nevertheless, we derive the IHL color-color relation using red giant stars ($3.6 < I_{\rm OGLE} - H_{\rm VVV} < 5.0; 17.0 < I_{\rm OGLE} < 19.5$) for validation of the color-color method. The relation and the $(I_{\rm OGLE} - H_{\rm VVV})_{\rm S}$ color in Section 4.2 suggest $(I_{\rm OGLE} - L_{Spitzer})_{\rm S} = 3.82 \pm 0.03$, which is in excellent agreement with the color measured from the model of $(I_{\rm OGLE} - L_{Spitzer})_{\rm S} = 3.81 \pm 0.02$.

4. PHYSICAL PARAMETERS: TWO LOW-MASS STARS IN THE GALACTIC BULGE

4.1. *OGLE-2017-BLG-1161L*

To derive the angular Einstein radius $\theta_{\rm E}$ for the lens by Equation (3), we estimate the angular radius θ_* of the source by locating it on a color-magnitude diagram (Yoo et al. 2004). We construct an $I-H$ versus I color-magnitude diagram by cross-matching the OGLE-IV I-band and the VVV (Saito et al. 2012) H-band stars within a $2' \times 2'$ square centered on the event (See Figure 3). We estimate the red giant clump to be $(I-H, I)_{\rm cl} = (4.59 \pm 0.02, 18.90 \pm 0.03)$ and find that the position of the source is $(I-H, I)_{\rm S} = (4.71 \pm 0.01, 18.70 \pm 0.03)$ from OGLE $I-$band data and CT13 $H-$band data aligned to the VVV magnitudes. From Nataf et al. (2016), we find that the intrinsic color and de-reddened magnitude of the red clump are $(I-H, I)_{\rm cl,0} = (1.30, 14.39)$. Thus, the intrinsic color and de-reddened brightness of the source are $(I-H, I)_{\rm S,0} = (1.42 \pm 0.03, 14.19 \pm 0.04)$. These values suggest the source is a K-type giant star (Bessell & Brett 1988). Using the color/surface-brightness relation of Adams et al. (2018), we obtain

$$\theta_* = 7.4 \pm 0.4\ \mu{\rm as}. \quad (8)$$

We derive the angular Einstein radius and the geocentric lens-source relative proper motion

$$\theta_{\rm E} = \frac{\theta_*}{\rho} = 0.159 \pm 0.009\ {\rm mas}; \quad (9)$$

$$\mu_{\rm rel} = \frac{\theta_{\rm E}}{t_{\rm E}} = 6.11 \pm 0.39\ {\rm mas\ yr^{-1}}. \quad (10)$$

Using Equation (1), we measure the lens mass,

$$M = \frac{\theta_{\rm E}}{\kappa\pi_{\rm E}} = \begin{cases} 0.51^{+0.12}_{-0.10} M_\odot \text{ for } \pi_{\rm E} \simeq 0.038 & (11) \\ 0.38^{+0.13}_{-0.12} M_\odot \text{ for } \pi_{\rm E} \simeq 0.051. & (12) \end{cases}$$

The lens-source relative parallax for the two cases is

$$\pi_{\rm rel} = \begin{cases} 0.0062 \pm 0.0014 \text{ for } \pi_{\rm E} \simeq 0.038 & (13) \\ 0.0083 \pm 0.0025 \text{ for } \pi_{\rm E} \simeq 0.051, & (14) \end{cases}$$

which are very small compared to the source parallax $\pi_{\rm S} \simeq 0.12$ (Nataf et al. 2016). Thus, the distance between the lens and the source is determined much more precisely than the distance to the lens or the source separately. We measure the lens-source distance,

$$D_{\rm LS} \simeq D_{\rm S}^2 \frac{\pi_{\rm rel}}{\rm AU} \begin{cases} 0.40 \pm 0.12 \text{ kpc for } \pi_{\rm E} \simeq 0.038 & (15) \\ 0.53 \pm 0.19 \text{ kpc for } \pi_{\rm E} \simeq 0.051, & (16) \end{cases}$$

where we adopt the source distance $D_{\rm S} = 8.0 \pm 0.8$ kpc using the Galactic model of Zhu et al. (2017). Because the lens-source distance is $\lesssim 1$ kpc and the source is almost certainly a bulge red-clump star, the lens should be an M/K dwarf in the Galactic bulge. We list the derived source star properties in Table 2 and the physical parameters of all the four-fold degenerate solutions in Table 3.

4.2. *OGLE-2017-BLG-1254L*

We construct an $I-H$ versus I color-magnitude diagram via the OGLE-IV I-band and the VVV H-band stars within a $2' \times 2'$ square centered on the event (See Figure 3). We measure the centroid of the red giant clump $(I-H, I)_{\rm cl} = (4.28 \pm 0.02, 18.39 \pm 0.03)$ and the position of the source $(I-H, I)_{\rm S} = (4.12 \pm 0.02, 18.53 \pm 0.01)$.

From Nataf et al. (2016), we find that the intrinsic color and de-reddened magnitude of the red clump are $(I-H, I)_{\rm cl,0} = (1.30, 14.35)$, from which we derive the intrinsic color and de-reddened brightness of the source are $(I-H, I)_{\rm S,0} = (1.14 \pm 0.03, 14.51 \pm 0.03)$. Thus, the source is a G-type giant star (Bessell & Brett 1988). Applying the color/surface-brightness relation of Adams et al. (2018), we obtain

$$\theta_* = 5.2 \pm 0.3\ \mu{\rm as}; \tag{17}$$

$$M_{\rm L} = \frac{\theta_{\rm E}}{\kappa \pi_{\rm E}} = 0.60 \pm 0.03 M_\odot; \tag{18}$$

$$D_{\rm LS} \simeq D_{\rm S}^2 \frac{\pi_{\rm rel}}{\rm AU} = 0.53 \pm 0.11\ {\rm kpc}, \tag{19}$$

where we also adopt the source distance $D_{\rm S} = 7.8 \pm 0.8$ kpc using the Galactic model of Zhu et al. (2017). Thus, the lens is probably a K dwarf in the Galactic bulge. We list the derived source star properties in Table 2 and the physical parameters of OGLE-2017-BLG-1254 in Table 3.

5. DISCUSSION AND CONCLUSION

We have reported the analysis of two microlensing events OGLE-2017-BLG-1161 and OGLE-2017-BLG-1254, each of which displays both finite-source effects detected by the ground-based data and the microlens parallax measured by the joint analysis of the ground-based data and the *Spitzer* data. Including these two events, the *Spitzer* microlensing program has measured the mass and distance for eight isolated objects from 2015–2017, yielding an estimate of the apparent detection frequency $\sim 8/328 = 2.4\%$[3]. This apparent frequency agrees with the theoretical frequency $\sim 3.3\%$ (Zhu et al. 2016) within 1σ for Poisson statistics. The theoretical frequency assumes that the probability to detect the finite-source effects in single-lens events is the same for ground and *Spitzer* observations, but the *Spitzer* data only detected finite-source effects for two events[4] (OGLE-2015-BLG-0763 (Zhu et al. 2016), OGLE-2015-BLG-1482 Chung et al. 2017), with a degeneracy in ρ. This is because the *Spitzer* observations only have a $\Gamma \sim {\rm day}^{-1}$ cadence and require a 3–10 day turnaround time after selection of the event, leading to the loss of finite-source effect detection from *Spitzer* observations.

The probability of finite-source effects occurring in a single-lens event is

$$P = \rho \equiv \frac{\theta_*}{\theta_{\rm E}}. \tag{20}$$

This, when combined with the microlensing rate $\Gamma_{\mu{\rm lens}} \propto n\mu_{\rm rel}\theta_{\rm E}$ (n is the number density), yields the finite-source event rate (Gould & Yee 2012; Shvartzvald et al. 2019)

$$\Gamma_{\rm FS} = \rho \Gamma_{\mu{\rm lens}} \propto n\mu_{\rm rel}\theta_*. \tag{21}$$

We apply the Galactic model described in Zhu et al. (2017) and estimate the probability density distribution of finite-source events based on $n \times \mu_{\rm rel}$. We average the distributions in the direction of the eight *Spitzer* finite-source events and assume the source distances are 8.3 kpc for all the events (following Zhu et al. 2017). For events with two degenerate solutions, both solutions are included at half the weight. Figure 4 compares the resulting probability densities for different masses and distances with the eight *Spitzer* finite-source events. Figure 5 and 6 compare the cumulative distributions of the lens distance and lens mass, respectively. In this comparison, we do not take into account the *Spitzer* detection efficiency, and possible selection or publication biases. Such detailed analysis is beyond the scope of this paper and will be done in future complete statistical analysis of the *Spitzer* campaigns.

The observed *Spitzer* sample agrees with expectations from the Galactic model. The distance distribution of the eight events is consistent with the Galactic model of Zhu et al. (2017) with a Kolmogorov-Smirnov probability of 30.3%, and the mass distribution is consistent with the initial mass function of Kroupa (2001) and Chabrier (2003) with a Kolmogorov-Smirnov probability of 84.9% and 72.3%, respectively. Both the Galactic model and the eight *Spitzer* events show that the finite-source effects have strong bias toward objects in the Galactic bulge. This is primarily because the stellar number density in the Galactic bulge is significantly higher than that of the Galactic disk, while the lens-source relative proper motions of disk lenses are only slightly higher on average (see Figure 1 and 2 of Zhu et al. 2017). In addition, the finite-source effects are biased toward the more common low-mass objects (M-dwarfs and brown dwarfs). However, *Spitzer* has no detection of a low-mass brown dwarf ($M_{\rm L} < 0.04 M_\odot$) in the Galactic bulge, in tension with the expectations from the Galactic model. This is likely due to the 3–10 day delay of the *Spitzer* observations, which is comparable to the typical microlens timescale for a bulge low-mass brown dwarf is less than 6 days.

Shan et al. (2018) compared 13 well-characterized *Spitzer* systems (10 binary/planetary lenses and 3 single lenses) with Bayesian predictions from Galactic models and found that they are in excellent agreement. Our preliminary comparison of eight *Spitzer* single lenses also suggests good agreement with the expectations from the Galactic model. Assuming the empirical rate from 2015–2017 season, we expect another 5–10 detections of finite-source events in 2018 and 2019 *Spitzer* microlensing campaigns, and thus future

---

[3] *Spitzer* observed 524 events from 2015–2017, but only 328 events are single-lens events with a clear *Spitzer* signal.

[4] For OGLE-2017-BLG-1186, the best-fit *Spitzer* light curve also shows finite-source effects, but the daily *Spitzer* data are insufficient for the detection.

statistical analyses of all *Spitzer* finite-source events will potentially allow a study of specific stellar populations and test the Galactic model.

W.Z., W.T., S.-S.L. and S.M. acknowledges support by the National Science Foundation of China (Grant No. 11821303 and 11761131004). This work is based (in part) on observations made with the *Spitzer* Space Telescope, which is operated by the Jet Propulsion Laboratory, California Institute of Technology under a contract with NASA. Support for this work was provided by NASA through an award issued by JPL/Caltech. The OGLE has received funding from the National Science Centre, Poland, grant MAESTRO 2014/14/A/ST9/00121 to AU. This research has made use of the KMTNet system operated by the Korea Astronomy and Space Science Institute (KASI) and the data were obtained at three host sites of CTIO in Chile, SAAO in South Africa, and SSO in Australia. The MOA project is supported by JSPS KAKENHI Grant Number JSPS24253004, JSPS26247023, JSPS23340064, JSPS15H00781, JP16H06287, and JP17H02871. The research has made use of data obtained at the Danish 1.54m telescope at ESOs La Silla Observatory. CITEUC is funded by National Funds through FCT - Foundation for Science and Technology (project: UID/Multi/00611/2013) and FEDER - European Regional Development Fund through COMPETE 2020 - Operational Programme Competitiveness and Internationalization (project: POCI-01-0145-FEDER-006922). Work by AG was supported by AST-1516842 from the US NSF and JPL grant 1500811. Wei Zhu was supported bythe Beatrice and Vincent Tremaine Fellowship at CITA. Work by CH was supported by the grant (2017R1A4A1015178) of National Research Foundation of Korea. YT acknowledges the support of DFG priority program SPP 1992 Exploring the Diversity of Extrasolar Planets (WA 1047/11-1). L.M. acknowledges support from the Italian Minister of Instruction, University and Research (MIUR) through FFABR 2017 fund.

REFERENCES

Adams, A. D., Boyajian, T. S., & von Braun, K. 2018, MNRAS, 473, 3608

Alard, C., & Lupton, R. H. 1998, ApJ, 503, 325

Albrow, M. D., Horne, K., Bramich, D. M., et al. 2009, MNRAS, 397, 2099

Alcock, C., Allsman, R. A., Alves, D., et al. 1995, ApJL, 454, L125

An, J. H., Albrow, M. D., Beaulieu, J.-P., et al. 2002, ApJ, 572, 521

Barclay, T., Quintana, E. V., Raymond, S. N., & Penny, M. T. 2017, ApJ, 841, 86

Bessell, M. S., & Brett, J. M. 1988, PASP, 100, 1134

Bond, I. A., Abe, F., Dodd, R. J., et al. 2001, MNRAS, 327, 868

Boyajian, T. S., van Belle, G., & von Braun, K. 2014, AJ, 147, 47

Bramich, D. M. 2008, MNRAS, 386, L77

Calchi Novati, S., Gould, A., Udalski, A., et al. 2015a, ApJ, 804, 20

Calchi Novati, S., Gould, A., Yee, J. C., et al. 2015b, ApJ, 814, 92

Chabrier, G. 2003, PASP, 115, 763

Chung, S.-J., Zhu, W., Udalski, A., et al. 2017, ApJ, 838, 154

Clanton, C., & Gaudi, B. S. 2017, ApJ, 834, 46

Claret, A., & Bloemen, S. 2011, A&A, 529, A75

DePoy, D. L., Atwood, B., Belville, S. R., et al. 2003, in Proc. SPIE, Vol. 4841, Instrument Design and Performance for Optical/Infrared Ground-based Telescopes, ed. M. Iye & A. F. M. Moorwood, 827–838

Dominik, M., Jørgensen, U. G., Rattenbury, N. J., et al. 2010, Astronomische Nachrichten, 331, 671

Dong, S., Udalski, A., Gould, A., et al. 2007, ApJ, 664, 862

Dong, S., Mérand, A., Delplancke-Ströbele, F., et al. 2019, ApJ, 871, 70

Fields, D. L., Albrow, M. D., An, J., et al. 2003, ApJ, 596, 1305

Foreman-Mackey, D., Hogg, D. W., Lang, D., & Goodman, J. 2013, PASP, 125, 306

Gould, A. 1992, ApJ, 392, 442

—. 1994, ApJL, 421, L75

—. 2000a, ApJ, 542, 785

—. 2000b, ApJ, 535, 928

—. 2004, ApJ, 606, 319

Gould, A., & Yee, J. C. 2012, ApJL, 755, L17

Gould, A., Udalski, A., Monard, B., et al. 2009, ApJL, 698, L147

Gould, A., Dong, S., Gaudi, B. S., et al. 2010, ApJ, 720, 1073

Griest, K., & Safizadeh, N. 1998, ApJ, 500, 37

Houdashelt, M. L., Bell, R. A., & Sweigart, A. V. 2000, AJ, 119, 1448

Kervella, P., & Fouqué, P. 2008, A&A, 491, 855

Kim, D.-J., Kim, H.-W., Hwang, K.-H., et al. 2018, AJ, 155, 76

Kim, S.-L., Lee, C.-U., Park, B.-G., et al. 2016, Journal of Korean Astronomical Society, 49, 37

Kroupa, P. 2001, MNRAS, 322, 231

Li, S.-S., Zang, W., Udalski, A., et al. 2019, arXiv e-prints, arXiv:1904.07718

Ma, S., Mao, S., Ida, S., Zhu, W., & Lin, D. N. C. 2016, MNRAS, 461, L107

Mao, S. 2012, Research in Astronomy and Astrophysics, 12, 947

Mao, S., Smith, M. C., Woźniak, P., et al. 2002, MNRAS, 329, 349

Mróz, P., Udalski, A., Skowron, J., et al. 2017, Nature, 548, 183

Mróz, P., Ryu, Y.-H., Skowron, J., et al. 2018, AJ, 155, 121

Mróz, P., Udalski, A., Bennett, D. P., et al. 2019, A&A, 622, A201

Nataf, D. M., Gonzalez, O. A., Casagrande, L., et al. 2016, MNRAS, 456, 2692

Nemiroff, R. J., & Wickramasinghe, W. A. D. T. 1994, ApJL, 424, L21

Paczyński, B. 1986, ApJ, 304, 1

Pfyffer, S., Alibert, Y., Benz, W., & Swoboda, D. 2015, A&A, 579, A37

Refsdal, S. 1966, MNRAS, 134, 315

Saito, R. K., Hempel, M., Minniti, D., et al. 2012, A&A, 537, A107

Schechter, P. L., Mateo, M., & Saha, A. 1993, PASP, 105, 1342

Shan, Y., Yee, J. C., Udalski, A., et al. 2018, arXiv e-prints, arXiv:1805.09350

Shin, I.-G., Udalski, A., Yee, J. C., et al. 2017, AJ, 154, 176

—. 2018, ApJ, 863, 23

Shvartzvald, Y., Yee, J. C., Skowron, J., et al. 2019, AJ, 157, 106

Sumi, T., Kamiya, K., Bennett, D. P., et al. 2011, Nature, 473, 349

Sumi, T., Udalski, A., Bennett, D. P., et al. 2016, ApJ, 825, 112

Udalski, A., Szymański, M. K., & Szymański, G. 2015a, AcA, 65, 1

Udalski, A., Yee, J. C., Gould, A., et al. 2015b, ApJ, 799, 237

Udalski, A., Ryu, Y.-H., Sajadian, S., et al. 2018, AcA, 68, 1

Veras, D., & Raymond, S. N. 2012, MNRAS, 421, L117

Witt, H. J., & Mao, S. 1994, ApJ, 430, 505

Wozniak, P. R. 2000, AcA, 50, 421

Wyrzykowski, Ł., Kostrzewa-Rutkowska, Z., Skowron, J., et al. 2016, MNRAS, 458, 3012

Yee, J. C., Udalski, A., Sumi, T., et al. 2009, ApJ, 703, 2082

Yee, J. C., Gould, A., Beichman, C., et al. 2015a, ApJ, 810, 155

Yee, J. C., Udalski, A., Calchi Novati, S., et al. 2015b, ApJ, 802, 76

Yoo, J., DePoy, D. L., Gal-Yam, A., et al. 2004, ApJ, 603, 139

Zhu, W., Udalski, A., Gould, A., et al. 2015, ApJ, 805, 8

Zhu, W., Calchi Novati, S., Gould, A., et al. 2016, ApJ, 825, 60

Zhu, W., Udalski, A., Calchi Novati, S., et al. 2017, AJ, 154, 210

Table 1. Best-fit parameters for OGLE-2017-BLG-1161 and OGLE-2017-BLG-1254 and their 68% uncertainty range from the MCMC

Event	OGLE-2017-BLG-1161				OGLE-2017-BLG-1254	
Solution	$(+,+)$	$(+,-)$	$(-,-)$	$(-,+)$	$(0,+)$	$(0,-)$
$t_{0,\oplus}$ -2450000(d)	7933.548(2)	7933.548(2)	7933.548(2)	7933.548(2)	7952.2519(4)	7952.2518(4)
$u_{0,\oplus}$	0.0214(8)	0.0214(9)	-0.0214(9)	-0.0214(9)	0.0003(10)	-0.0003(9)
$t_{\rm E}$	9.5(3)	9.5(3)	9.5(3)	9.4(3)	15.43(6)	15.42(7)
ρ)	0.0464(15)	0.0465(15)	0.0467(15)	0.0466(16)	0.0251(1)	0.0251(1)
$\pi_{\rm E,N}$	-0.000(23)	-0.034(21)	-0.000(22)	0.037(22)	0.0203(7)	-0.0174(7)
$\pi_{\rm E,E}$	0.039(7)	0.038(5)	0.038(5)	0.037(6)	0.0368(4)	0.0384(5)
$\pi_{\rm E}$	0.039(9)	0.051(17)	0.038(8)	0.052(16)	0.0420(7)	0.0421(7)
$I_{\rm s,OGLE}$	18.71(3)	18.70(3)	18.70(3)	18.70(3)	18.53(1)	18.53(1)
$I_{\rm b,OGLE}$	18.71(3)	18.72(3)	18.72(3)	18.72(3)	21.32(6)	21.32(6)
$\chi^2_{\rm penalty}$	0.00	0.02	0.01	0.02	-	-
χ^2/dof	618.41/617	618.35/617	618.25/617	618.30/617	8254.78/8256	8254.69/8256

Table 2. Derived Source Star Properties for OGLE-2017-BLG-1161 and OGLE-2017-BLG-1254.

Parameters	Units	Value	
		OGLE-2017-BLG-1161	OGLE-2017-BLG-1254
A_I	[mag]	~ 4.5	~ 4.2
$I_{\rm S}$	[mag]	18.70 ± 0.03	18.53 ± 0.01
$H_{\rm S}$	[mag]	13.99 ± 0.03	14.41 ± 0.01
$(I-H)_{\rm S}$		4.71 ± 0.01	4.12 ± 0.02
$(I-L)_{\rm S}$		4.55 ± 0.02	3.81 ± 0.02
$I_{\rm S,0}$	[mag]	14.19 ± 0.04	14.51 ± 0.03
$H_{\rm S,0}$	[mag]	12.77 ± 0.04	13.37 ± 0.03
$(I-H)_{\rm S,0}$		1.42 ± 0.03	1.14 ± 0.03
θ_*	[μas]	7.4 ± 0.04	5.2 ± 0.03

Table 3. Physical parameters for OGLE-2017-BLG-1161 and OGLE-2017-BLG-1254.

Event	OGLE-2017-BLG-1161				OGLE-2017-BLG-1254
Solution	$(+,+)$	$(+,-)$	$(-,-)$	$(-,+)$	$(0,+)$ and $(0,-)$
$\theta_{\rm E}$ [mas]	0.159 ± 0.009	0.159 ± 0.009	0.159 ± 0.009	0.159 ± 0.009	0.207 ± 0.008
$M_{\rm L}$ [$M_\odot$]	$0.50^{+0.12}_{-0.10}$	$0.38^{+0.13}_{-0.12}$	$0.51^{+0.11}_{-0.10}$	$0.38^{+0.12}_{-0.11}$	0.60 ± 0.03
$D_{\rm LS}$ [kpc]	0.40 ± 0.12	0.53 ± 0.19	0.40 ± 0.12	0.53 ± 0.19	0.53 ± 0.11
$\mu_{\rm rel}$ [mas yr^{-1}]	6.11 ± 0.39	6.11 ± 0.39	6.11 ± 0.39	6.11 ± 0.39	4.90 ± 0.20

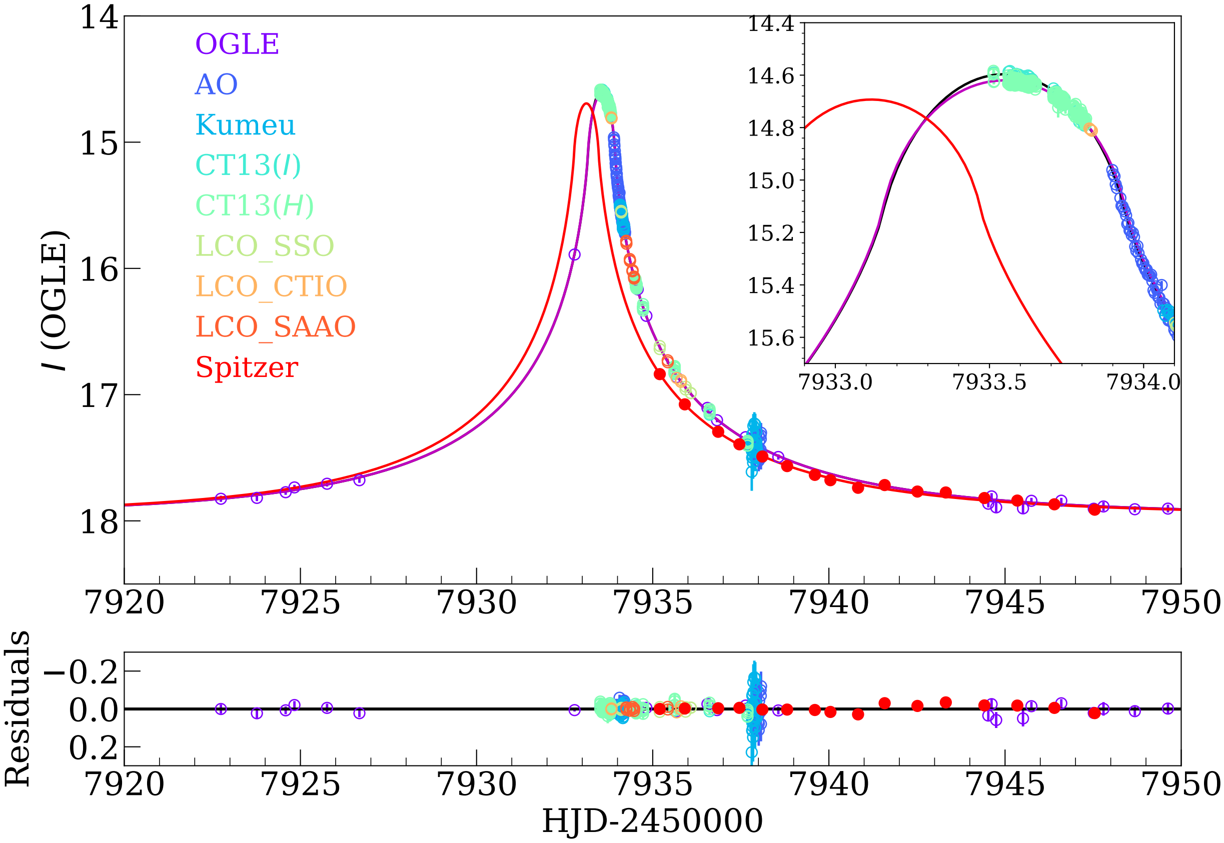

Figure 1. The light curves of event OGLE-2017-BLG-1161. The black and magenta lines represent the best-fit $(-,+)$ model for the ground data with I and H band, respectively, and the red line shows the corresponding model for *Spitzer*. The inset in the top panel shows the peak of the event, with a clear finite-source effect. The circles with different colors are ground-based data points from different collaborations or bands. The red dots are *Spitzer* data points.

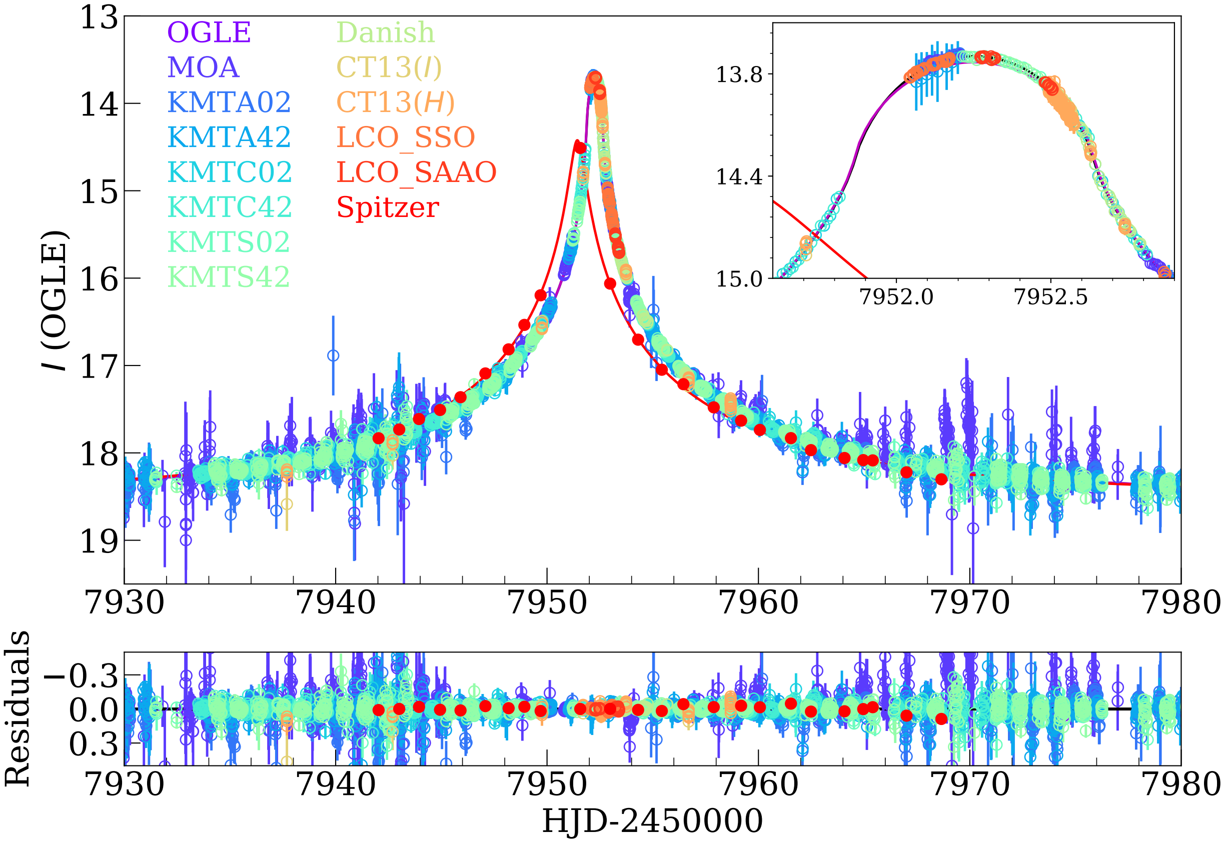

Figure 2. Ground-based and Spitzer data and best-fit model light curves of event OGLE-2017-BLG-1254 for the $(0,+)$ model. Symbols are similar to those in Figure 1.

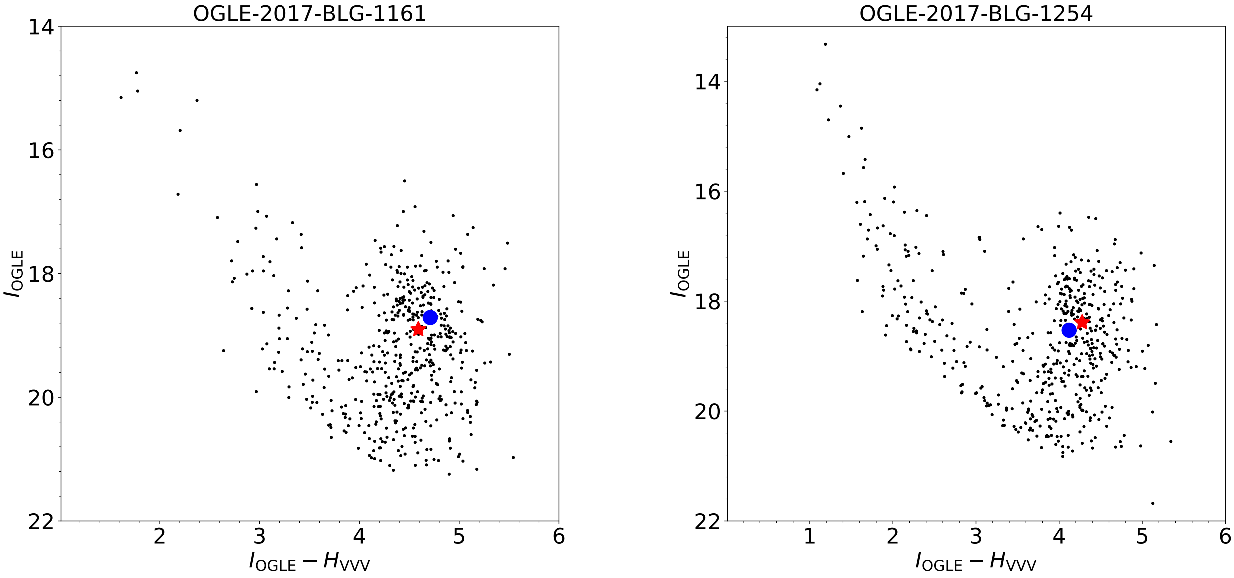

Figure 3. OGLE-VVV color-magnitude diagrams of a $2' \times 2'$ square centered on OGLE-2017-BLG-1161 (left panel) and OGLE-2017-BLG-1254 (right panel). The red asterisks show the centroid of the red clump. The blue dots indicate the position of the source.

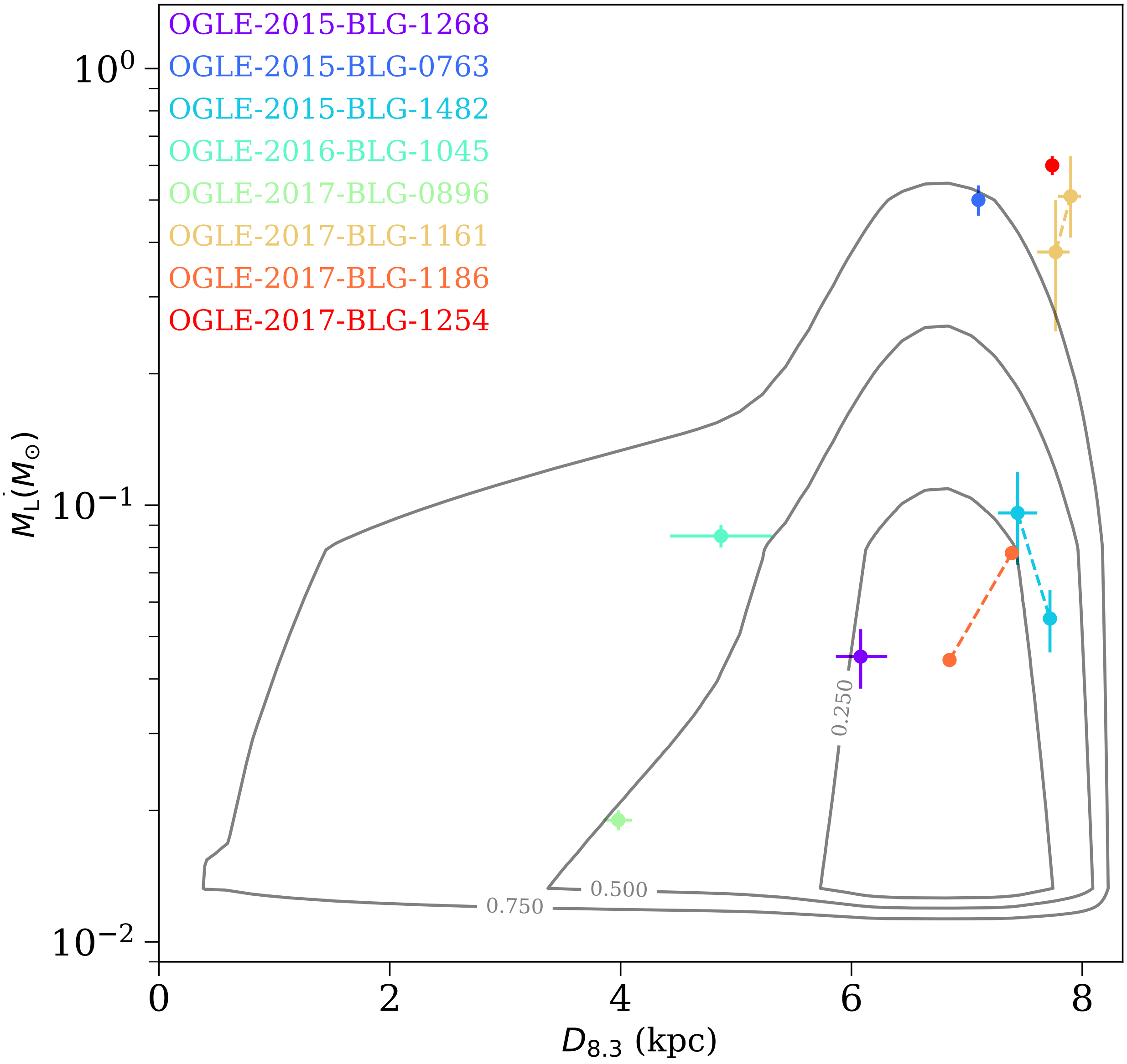

Figure 4. Bayesian probability density distributions from the Galactic model of Zhu et al. (2017) compared to the eight published *Spitzer* finite-source events. We fix the source distance to 8.3 kpc and then derive the lens distance $D_{8.3}$ for all the events. The predicted mass distribution is derived from the initial mass function of Kroupa (2001). The dots with different colors represent different events. The two dots connected by dash lines represent the two degenerate solutions of one event. The grey lines represent equal probability density. The values on the contours indicate the total probability inside the contours predicted by the Galactic model and the total probability is normalized to unity.

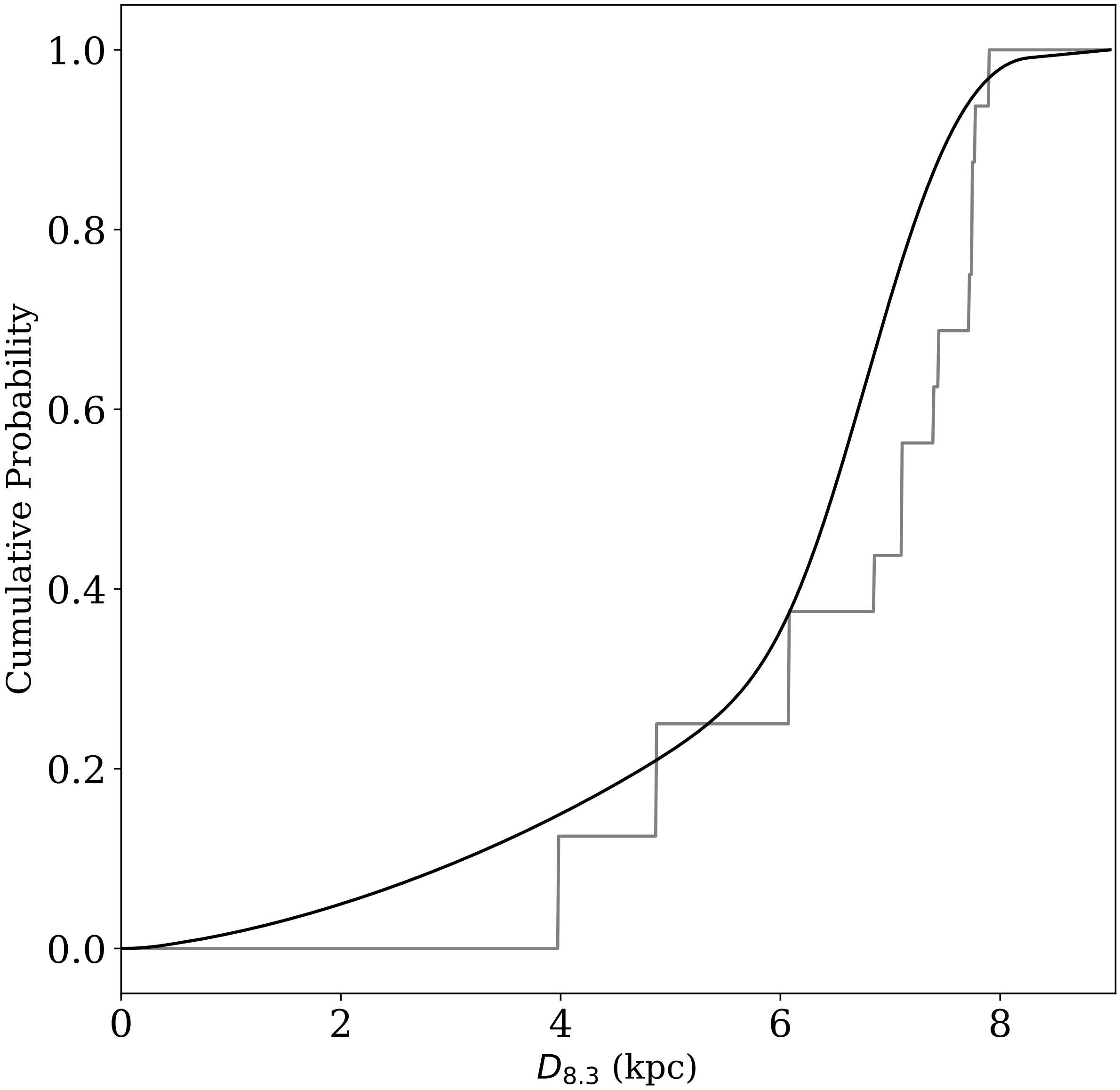

Figure 5. Cumulative distribution of the lens distance from the Galactic model of Zhu et al. (2017) and the eight published *Spitzer* finite-source events. We fix the source distance of 8.3 kpc and then derive the lens distance $D_{8.3}$ for all the events. The black line represents the distribution predicted by the Galactic model, and the grey lines represents the distribution calculated from the eight events. The observed distribution is consistent with the Galactic model with a Kolmogorov-Smirnov probability of 30.3%.

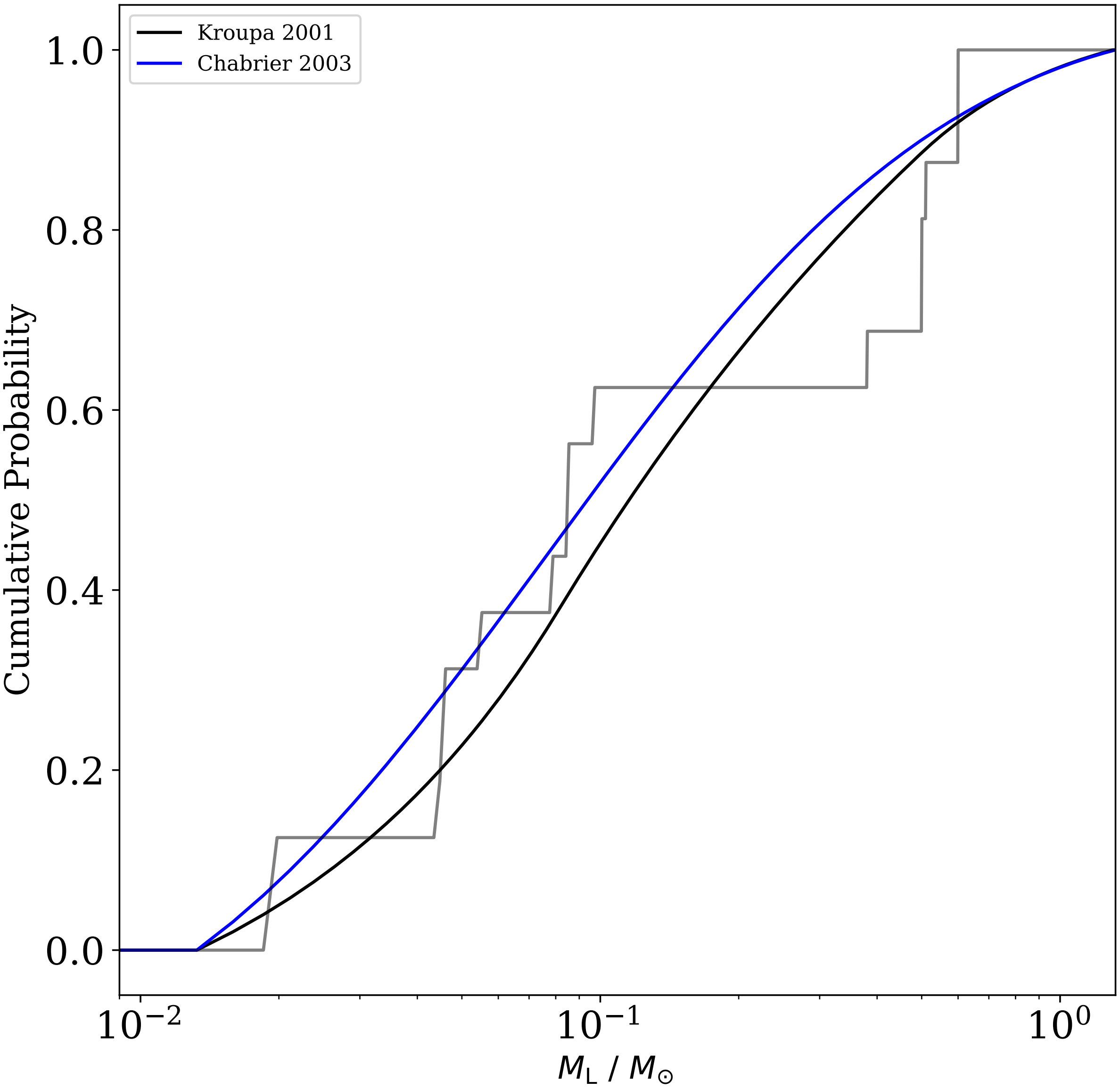

Figure 6. Cumulative distribution of the lens mass from the initial mass function and the eight published *Spitzer* finite-source events. The black line represents the distribution predicted by the initial mass function of Kroupa (2001) and the blue line represents the distribution calculated from Chabrier (2003). The observed distribution is consistent with the initial mass functions of Kroupa (2001) and Chabrier (2003) with a Kolmogorov-Smirnov probability of 84.9% and 72.3%, respectively.